High-resolution whole-genome analysis of sister-chromatid contacts

Elena Espinosa, Evelyne Paly, François-Xavier Barre

Version of Record: https://www.sciencedirect.com/science/article/pii/S1097276520304354
Manuscript_7257f32fa2fae80a6fd54d3a538976b2

High-resolution whole-genome analysis of sister-chromatid contacts

Elena Espinosa[1], Evelyne Paly[1] and François-Xavier Barre[1*]

* **Lead Contact:** francois-xavier.barre@i2bc.paris-saclay.fr

[1]Institute for Integrative Biology of the Cell (I2BC), Université Paris-Saclay, CEA, CNRS, Université Paris Sud, 1 Avenue de la Terrasse, 91198 Gif-sur-Yvette, France

Summary

Sister-chromatid cohesion describes the orderly association of newly-replicated DNA molecules behind replication forks. It plays an essential role in the maintenance and faithful transmission of genetic information. Cohesion is created by DNA topological links and proteinaceous bridges, whose formation and deposition could be potentially affected by many processes. Current knowledge on cohesion has been mainly gained by fluorescence microscopy observation. However, the resolution limit of microscopy and the restricted number of genomic positions that can be simultaneously visualized considerably hampered progress. Here we present a High-throughput methodology to monitor Sister Chromatid Contacts (Hi-SC2). Using the multi-chromosomal *Vibrio cholerae* bacterium as a model, we show that Hi-SC2 permits to monitor local variations in sister-chromatid cohesion at a high resolution over a whole genome.

Introduction

During replication, sister DNA copies emerging from a replication fork are orderly associated by the formation of DNA topological links and proteinaceous bridges. The phenomenon is referred to as sister-chromatid cohesion. In eukaryotes, cohesion is principally mediated by an evolutionarily-conserved multi-subunit complex, the cohesin (Haering et al., 2008; Nasmyth and Haering, 2009). Cohesins facilitate homology search for recombinational repair in interphase and ensure the proper attachment of chromosomes to the mitotic spindle for their faithful segregation in mitosis (Morales and Losada, 2018). In addition, they form intramolecular loops, which participate to the overall organization of the genome (Lazar-Stefanita et al., 2017; Morales and Losada, 2018; Schalbetter et al., 2017). In contrast, cohesion in bacteria is thought to mainly result from the formation of catenation links during replication, which can be locally modulated by DNA binding proteins (Joshi et al., 2013; Lesterlin et al., 2012; Nolivos et al., 2016; Wang et al., 2008). The basis for chromosome segregation in bacteria remains a matter of debate. However, it was proposed that local building and sudden release of tension in regions that exhibit prolonged juxtaposition of sister loci participated in segregation (Bates and Kleckner, 2005; Joshi et al., 2011). In addition, cohesion was shown to facilitate the repair of genetic lesions by homologous recombination and that topological cohesion is rapidly substituted by proteinaceous bridges in SOS conditions (Vickridge et al., 2017).

Fluorescence microscopy observation of bulk DNA and of a few genomic positions in a few cellular models suggested that the duration of cohesion varied according to genomic position (Haering et al., 2008). However, the resolution limit of microscopy and the restricted number of genomic positions that can be simultaneously visualized hampered the analysis of the many different processes that can influence the cohesiveness of newly-replicated DNA molecules. Two Conformation Capture (3C)-based techniques were recently developed to map sister-

chromatid interactions over a whole genome (Mitter et al., 2020; Oomen et al., 2020). The 3C methodology consists in fixing the intracellular conformation adopted by the chromosomes with a crosslinking agent before fragmentation with a restriction enzyme. The relative efficiency with which two different DNA fragments can be ligated then serves as a measure of their spatial proximity in the cell (Dekker et al., 2002). However, the presence of self-ligated or un-ligated products prevent mapping interactions between positions separated by less than 1500 bp (Lajoie et al., 2015). Thus, 3C-based methodologies cannot provide data on the frequency of contacts between the exact sister copies of a locus, calling for an alternative complementary method.

Here, we present a High-throughput methodology to monitor the relative frequency of Contacts between Sister Copies emerging from a replication fork (Hi-SC2). Using *Vibrio cholerae* as a model, we show that Hi-SC2 permits to analyse locus-specific variations in sister-chromatid cohesion over the entire length of chromosomes at an unprecedented resolution. *V. cholerae* carries homologues of most of the chromosome replication, maintenance and segregation machineries of *Escherichia coli*, the only organism in which cohesion was extensively investigated so far (Bates and Kleckner, 2005; Heidelberg et al., 2000; Joshi et al., 2013; Stouf et al., 2013). However, the genome of *V. cholerae* is divided on two circular chromosomes, Chr1 and Chr2, whereas *E. coli* harbours a single circular chromosome (Trucksis et al., 1998; Yamaichi et al., 1999). Chr1 derives from the mono-chromosomal ancestor of *E. coli* and *V. cholerae.* Chr2 derives from a domesticated mega-plasmid. The organisation and positioning of Chr2 nevertheless participate to the cell cycle of the bacterium (Galli et al., 2016). Chr1 and Chr2 harbour a single origin of bi-directional replication, *ori1* and *ori2*, respectively. Chr1 and Chr2 replication terminates in a region opposite of their origins, next to a site dedicated to the resolution of topological problems due to their circularity, *dif1* and *dif2*, respectively (Galli et al., 2019; Val et al., 2008). *V. cholerae*

is the agent of the deadly human disease cholera. However, most strains of *V. cholerae* are not pathogenic or only cause local outbreaks of gastroenteritis. Epidemic strains have so far been found in only 2 out of >200 possible somatic O-antigens serogroups (Chatterjee and Chaudhuri, 2003). They are characterized by the capacity to produce cholera toxin, which is responsible for the diarrhoea associated with the disease, and by the formation of Type IV toxin-coregulated pili (TCP), which are essential for small intestine colonization (Herrington et al., 1988). Both virulence factors are acquired by horizontal gene transfer. Cholera toxin is encoded in the genome of a lysogenic phage, CTXΦ (Val et al., 2005; Waldor and Mekalanos, 1996), which almost always integrates behind a Toxin Linked Cryptic satellite phage, TLCΦ, at the *dif1* locus (Hassan et al., 2010; Midonet et al., 2014, 2019). TCP is encoded in a 39.5 kbp vibrio pathogenicity island harboured by Chr1, VPI-1. Hi-SC2 revealed that cohesion is highly prolonged in large genomic territories centred on the replication origin and terminus regions of Chr1 and Chr2. It further revealed that the H-NS nucleoid-structuring protein, which acts as a transcriptional repressor of horizontally-acquired elements (Dorman, 2007), dramatically extends the duration of cohesion within VPI-1 and the O-antigen region (Ayala et al., 2015). Finally, Hi-SC2 unveiled small locus-specific variations in the duration of cohesion over the whole length of chromosomes, which had so far escaped scrutiny.

Design

Hi-SC2 exploits paired-end deep-sequencing to determine in parallel the status and position of sister-chromatid contact reporters inserted at random positions in a library of cells (Figure 1A). The SC2 reporters are short recombination cassettes for a topology-independent site-specific recombinase. The cassettes are composed of two directly-repeated recombination sites separated by a DNA segment too short to permit their excision by intramolecular recombination (Figure 1A). However, intermolecular recombination events between sister copies of a cassette can lead to the formation of a copy with a single recombination site on

one of the two sister chromatids and a copy with three recombination sites on the other chromatid (Figure 1A). The copy harbouring three recombination sites is subsequently converted into a copy with a single recombination site by intramolecular recombination (Figure 1A). Hence, the frequency of formation of cassettes with a single recombination site, hereafter referred to as the excision frequency, reflects the frequency of contacts between sister copies of the genomic position where the SC2 reporter was inserted (Figure 1A). Thus, Hi-SC2 is ideally suited to analyse the length of time during which sister copies of a locus remain in close proximity after replication. In brief, Hi-SC2 starts with the engineering of a cell line with a conditional expression allele for a site-specific recombinase and the creation of a library of cells harbouring a cognate SC2 reporter at different genomic positions. Production of the recombinase is induced for different lengths of time during cell growth and/or at specific stages of the cell cycle. The positions of SC2 reporters and the status of their recombination cassette are then determined by high-throughput paired-end sequencing (Figure 1A and Figure S1).

Results

Application of Hi-SC2 to V. cholerae

As a proof of principle, we applied Hi-SC2 to *V. cholerae*. To this end, we engineered EEV29, an El Tor N16961 *V. cholerae* strain harbouring an inducible allele of Cre, the tyrosine recombinase of phage P1. Cre acts on a specific 34 bp site, *loxP*. Previous work indicated that it cannot catalyse intramolecular recombination events between *loxP* sites separated by 21 bp, suggesting that a short recombination cassette composed of two directly-repeated *loxP* sites at such a distance could be used as a SC2 reporter (Hoess et al., 1985; Lesterlin et al., 2012). We also designed a reporter to detect the ability of Cre to access DNA and promote recombination events along the *V. cholerae* genome. The Cre-activity reporter consists of a long recombination cassette in which two directly-repeated *loxP* sites are

separated by 205 bp, which permits intramolecular recombination. Reporters were inserted at the extremity of a Mariner transposon specifically designed for efficient Tn-seq analysis (Figure S1A and S1B; (van Opijnen et al., 2009)). The transposon was used to generate cell libraries containing $>10^5$ clones (Table S1). Mariner transposons target 5'-TA-3' sites, which are distributed in average every 14 and 15 bp on Chr1 and Chr2 (Figure S1C). High-throughput sequencing permitted to verify that the reporters were randomly inserted at 5'-TA-3' sites without any orientation bias (Table S2) and that they were fairly distributed over the whole *V. cholerae* genome in each library (Figure S1D). The average distance between two reporters in the different libraries was less than 24 bp (Table S2 and Figure S1E). $\sim 10^7$ sequencing reads were enough to analyse the position and recombination status of 1000 reporters per kbp (Table S2). The read depth was lower at 14 loci, which corresponded to large essential gene operons, such as the cell division protein operon, and large repeated sequences such as ribosomal DNA regions (Table S3 and Figure S1D).

The excision frequency of a cassette, f_{exc}, can be analysed at different scales of precision, from large 100 kbp windows down to the exact location of the reporter (Figure 1B). Unless stated otherwise, we present f_{exc} profiles calculated over 10 kbp sliding-windows because it permits to highlight both short-range and long-range variations in f_{exc} along the whole length of the two *V. cholerae* chromosomes in small figures (Figure 1B). By convention, f_{exc} profiles are shown in a clockwise orientation starting from the origin of replication of the chromosomes (Figure 1B).

The f_{exc} of short *loxP* cassettes reflects the frequency of sister-chromatid contacts

No excision of short and long *loxP* cassettes occurred before the induction of Cre production and their f_{exc} increased as a function of time, suggesting that excision events exclusively resulted from Cre-mediated recombination (Figure 2A). Correspondingly, the f_{exc} profiles of

short *loxP* cassettes were identical in EEV29 and EEV174, a Δ*recA* derivative of EEV29 (Figure S2A).

The f_{exc} of short cassettes varied between ~20% and ~70% after 90' of Cre production in slow growth conditions (Figure 2A). Independent short cassette reporter libraries yielded identical f_{exc} profiles, demonstrating the robustness of the technique (Figure 2B). In contrast, the f_{exc} of long cassettes was constant over the whole length of the two *V. cholerae* chromosomes, reached 80% after only 30'of Cre production and almost 100% after 60' in slow growth conditions, demonstrating that local variations in the f_{exc} of short *loxP* cassettes were not due to differences in the accessibility of DNA and/or the activity of Cre along the genome (Figure 2A).

The f_{exc} profile of short *loxP* cassettes was higher in fast growth conditions than in slow growth conditions. i.e. in conditions in which a higher number of replication rounds is reached, in agreement with the hypothesis that they resulted from recombination events between sister chromatids (Figure S2B). To confirm this hypothesis, we followed the f_{exc} of short cassettes in cells treated with rifampicin, which impedes the initiation of Chr1 replication without preventing the advance of replication forks in cells in which replication was initiated before its addition (Figure 3A, (Rasmussen et al., 2007)). Rifampicin does not directly affect the initiation of Chr2 replication (Figure 3A, (Rasmussen et al., 2007)). However, new rounds of Chr2 replication will eventually cease because the initiation of Chr2 replication depends on the duplication of a sequence located on Chr1, *crtS* (Figure 3A, (Baek and Chattoraj, 2014; Val et al., 2016)). As a result, the proportion of cells harbouring two copies the terminus regions of the 2 chromosomes initially increases with time after addition of rifampicin (Figure 3A). Likewise, the proportion cells harbouring two *crtS* copies initially increases, leading to the initiation of a few more rounds of Chr2 replication (Figure 3A). As rifampicin inhibits transcription, expression of the *cre* gene was induced 10' before its

addition. It was sufficient to achieve >30% and >60% of excision of the long cassettes after 20' and 40' of growth in the presence of rifampicin, respectively (Figure S3). In contrast, rifampicin drastically reduced the f_{exc} of short cassettes (Figure 3B). The f_{exc} was below 0.1% in the middle of the replication arms of the two chromosomes (Figure 3B). It was higher near *ori2* and near *dif1* and *dif2*, as expected from the mode of action of rifampicin in *V. cholerae* (Figure 3B).

Taken together, these results demonstrate that the f_{exc} of short *loxP* cassettes exclusively results from Cre-mediated recombination, that its variations are not due to differences in the accessibility or activity of Cre along the genome and are mainly due to intermolecular recombination events between sister chromatids. Thus, the f_{exc} of short *loxP* cassettes reflects the relative frequency of sister-chromatid contacts, f_{SC2}, at their position of insertions.

Cre-based f_{SC2} measurements report the extent of cohesion

The f_{exc} of short *loxP* cassettes was strikingly elevated in five large 200 kbp genomic territories corresponding to the replication origin and replication terminus of each of the two *V. cholerae* chromosomes and to the middle of the left replication arm of Chr1 (Figure 2A and B). The high f_{SC2} in these regions could be due a longer duration of the orderly association of newly-replicated DNA behind the replication forks, i.e. prolonged cohesion, but also to replication initiation and termination processes, to a slower speed of replication forks, and/or to the spatial confinement of individualised sister DNA copies in the same cellular compartment when cohesion has been released.

Marker frequency analysis of an asynchronous population of cells under steady state growth showed that the average speed of replication is constant along the two *V. cholerae* chromosomes, suggesting that local differences in the speed of replication were unlikely to participate to the formation of the five large domains with a high f_{SC2} (Figure S4, (Galli et al., 2019)).

In *V. cholerae*, as in most bacteria studied so far, replication and segregation are concurrent (Espinosa et al., 2017). Fluorescence microscopy analysis showed that Chr1 and Chr2 are both longitudinally arranged. In new born cells, *ori1* locates at the old pole, *ori2* at mid-cell and *dif1* and *dif2* at the new pole (Figure 4A, (David et al., 2014)). It further revealed that sister copies of loci along the major part the two *V. cholerae* chromosomes, including *ori1*, *ori2* and the middle of the left arm of Chr1, migrate toward opposite cell poles after their individualisation (Figure 4A, (David et al., 2014)). Thus, they are spatially separated. In contrast, the terminus regions of both Chr1 and Chr2 were found to be confined to mid-cell until the initiation of cell division (Figure 4A, (David et al., 2014; Demarre et al., 2014; Galli et al., 2017)).

To differentiate the contributions of cohesion, of the replication initiation and termination processes and of the spatial confinement of individualised sister DNA to the f_{SC2}, we applied the Hi-SC2 methodology to MCH1, a synthetic mono-chromosomal derivative of El Tor N16961, in which Chr2 was integrated in the replication terminus of Chr1 (Val et al., 2012). The right and left part of the terminus region of Chr1 are fused to the right and left part of the *ori2* region in the MCH1 chromosome (Figure 4B). Marker frequency analysis of a population of MCH1 cells under steady state growth showed that replication initiates at *ori1* and terminates near *dif2* (Galli et al., 2016). Fluorescence microscopy analysis further revealed that sister copies of the *dif1-ori2* fusions separate before sister copies of the *dif2* region and that they migrate to opposite sides of the cell division septum (Figure 4B, (Galli et al., 2016)). Nevertheless, the f_{exc} of short *loxP* cassettes at the *dif1-ori2* junctions was as high as the f_{exc} of short *loxP* cassettes within the *dif2* region (Figure 4C). Furthermore, the f_{exc} profile of the two parts of the *dif1*-territory in MCH1 was equivalent to the f_{exc} profile of the *dif1*-territory in EEV29 (Figure 4D). Finally, the high f_{exc} of short *loxP* cassettes in the *ori2*-territory was not entirely lost in MCH1 (Figure 4E).

Taken together, these observations suggest that variations in the speed of replication forks, replication initiation and termination processes and spatial confinement of individualised sister DNA copies in the same cellular compartment after the release of cohesion do not contribute to the elevated f_{SC2} near the origin and terminus of the two *V. cholerae* chromosomes nor to the elevated f_{SC2} in the middle of the left replication arm of Chr1. We conclude that Cre-based f_{SC2} measurements report the extent of cohesion.

Sister copy contacts in the terminus regions are lost prior to septum constriction

Previous fluorescence observations demonstrated that sister copies of *dif1* and *dif2* remain associated until the initiation of cell division, which suggested that sister copies of the replication termini were still cohesive at this stage of the cell cycle (Demarre et al., 2005; Galli et al., 2017). To check this possibility, we used a SC2 reporter based on a site-specific recombination machinery whose activity is restricted to the immediate vicinity of the cell division machinery and to the time of constriction, Xer, to analyse the f_{SC2} in terminus region of Chr1 and Chr2 during septum constriction (Demarre et al., 2014; Kennedy et al., 2008; Val et al., 2008). At this stage of the cell cycle, the f_{exc} of Xer-based SC2 reporters was null at all genomic positions but the terminus regions, in agreement with the ordered choreography of segregation of Chr1 and Chr2 and the temporal restriction of the activity of Xer (Figure 4F). The f_{exc} of Xer-based SC2 reporters remained very low over the whole *dif2*-territory, including the *dif2* position, and over most of the *dif1*-territory (Figure 4F). However, it was as high as the f_{exc} of short *loxP* cassettes in the immediate vicinity of *dif1* (Figure 4F). We conclude that most of the links between sister copies of the replication terminus of the two *V. cholerae* chromosomes are released prior to the initiation of cell division, with the exception of the immediate vicinity of *dif1*.

VPI-1 is at the centre of a highly cohesive territory

The large 200 kbp territory in the middle of the left replication arm of Chr1 where the f_{SC2} was elevated is centred on VPI-1 (Figure 5A and Figure S5A). Deletion of VPI-1 supressed the high f_{exc} of short *loxP* cassettes within the whole territory, without affecting the f_{exc} in the rest of the genome (Figure 5A and Figure S5A). These results prompted us to use fluorescence microscopy to inspect the segregation of a locus within the VPI-1 territory, L1, with respect to the segregation of a locus immediately downstream of it on the same replication arm, L2, with a lower f_{SC2} (Figure 5B). As a comparison, we analysed the relative segregation of two genomic positions in the right replication arm, R1 and R2, which are located at approximately the same distance from *ori1* than L1 and L2 and for which the f_{SC2} was equivalent (Figure 5B). We observed more cells with two R1 foci and a single R2 focus than cells with a single R1 focus and two R2 foci, as expected from the earlier replication of R1 (left panel of Figure 5C and Figure S5D). In contrast, there were more cells with a single L1 focus and two L2 foci than cells with two L1 foci and a single L2 focus, demonstrating that the separation of sister L1 copies was delayed compared to the separation of sister L2 copies, in agreement with the higher f_{SC2} at L1 compared to L2 (middle panel of Figure 5B and Figure S5D). Furthermore, we found that deletion of VPI-1 alleviated the segregation delay of sister L1 copies (right panel of Figure 5C and Figure S5D). Together, these results demonstrate that VPI-1 creates a highly cohesive territory.

The Histone-like Nucleoid Structuring protein promotes cohesion

The Histone-like Nucleoid Structuring protein, H-NS, acts as a transcriptional repressor in horizontally-acquired elements (Dorman, 2007). It notably regulates the virulence of *V. cholerae* and covers the VPI-1 and O-antigen regions (Figure 6A, bottom panel; Ayala et al., 2015; Chun et al., 2009; Herrington et al., 1988). Deletion of *hns* suppressed the high f_{exc} of short *loxP* cassettes within the 100 kbp origin-proximal part of the VPI-1 territory and within the O-antigen region without affecting the f_{exc} in the surrounding regions (upper panel of

Figure 6A, Figure 6B and Figure S6). We can exclude that H-NS promotes artefactual intramolecular excision of the short *loxP* cassettes because only one H-NS dimer unit can bind to the 21 bp DNA fragment separating the two *loxP* sites cassette (Amit et al., 2003) whereas 10 dimer units are required to induce 180° turns (Spurio et al., 1997). In addition, H-NS preferentially binds curved AT-rich sequences, which is not the case for the recombination cassettes and the 1500 bp transposition fragment within which they are inserted (Rimsky et al., 2001). Finally, 3C-analysis in *E. coli* indicated that deletion of H-NS promotes an increase in short-range intramolecular DNA contacts, which is the opposite effect of what we observed with Hi-SC2 (Lioy et al., 2018). Together, these results suggest that H-NS acts as a region-specific cohesion factor (upper panel of Figure 6A, Figure 6B and Figure S6).

Hi-SC2 unveiled small locus-specific variations in the duration of cohesion

Small short-distance (<10 kbp) fluctuations are superimposed on the large long-distance variations of the f_{exc} of short *loxP* cassettes (Figure 2B). They can be highlighted by plotting the difference between the 10 kbp f_{exc} profile and the 100 kbp f_{exc} profile (Figure 7A). It revealed that they were highly reproducible (Figure 7A). Note, however, that they vary with the growth conditions, suggesting that they are linked to physiological parameters (Figure S2B). We then inspected if small locus-specific variations in the f_{SC2} were related to specific features of the genome. An obvious candidate was the local base pair composition of the chromosomes, which can influence the binding of proteins that affect cohesion, such as H-NS (Figure 6). However, we did not observe any correlation between the short-distance f_{exc} profile and the local variations in the base pair composition of the chromosomes (Figure 7B). Previous work in *E. coli* indicated that the elevated cohesion of two regions close to origin of replication of the chromosome was linked to a high density of 5'-GATC-3' motifs, the actin site of the Dam methylase (Joshi et al., 2013). The genome of *V. cholerae* encodes for a

homolog of the *E. coli* Dam methylase, which is essential (Adhikari and Curtis, 2016; Marinus and Casadesus, 2009). We observed a possible positive correlation between the density of GATC motifs and local variations in the f_{SC2} in two positions in immediate proximity of the origin of replication of Chr1 (Figure S7). However, the correlation was not quantitative and was absent in most of the genome (Figure7C and Figure S7). In particular, we observed an elevated cohesion in regions with a low density of GATC sites, such as the O-antigen region, VPI-1 and the other genomic islands (Figure 7C and Figure S7). Finally, it was previously proposed that transcription could influence of cohesion by promoting the formation of topological links. However, we did not observe any global correlation between the local variations of the f_{SC2} and the transcriptional level (Figure 7D, (Mandlik et al., 2011)).

Discussion

The three-dimensional cellular arrangement of chromosomes is crucial for the regulation, maintenance and inheritance of the genetic material. It was initially studied by microscopy, which has a limited resolution and only permits the simultaneous observation of a restricted number of genomic loci. Considerable progress was made in the past decades thanks to the development of Chromosome Conformation Capture (3C) techniques (Dekker et al., 2002; Lieberman-Aiden et al., 2009) and molecular genetic approaches based on the specific properties of some transposases (DeBoy and Craig, 1996; Walker et al., 2020) and site-specific recombinases (Higgins et al., 1996; Mercier et al., 2008; Valens et al., 2004). However, the interaction between sister chromatids in the cell cycle and in particular their orderly association behind replication forks remained elusive. Here we describe a high-throughput methodology to monitor the relative frequency of Contacts between Sister Copies of a genomic position, Hi-SC2. The approach relies on the generation of a library of cells harbouring SC2 reporters at different genomic positions and deep sequencing to determine the

position and status of the reporters (Figure 1). The SC2 reporters are composed of two-directly repeated sites for a topology independent recombinase, which are close enough to prevent intramolecular recombination. However, when sister copies of the cassette remain in close proximity after replication, intermolecular recombination events can lead to cassette excision events. Hence, the f_{exc} of the recombination cassettes reflects the relative frequency of contacts between sister copies of the genomic position where the SC2 reporter was inserted, f_{SC2} (Figure 2 and 3). Thus, Hi-SC2 is perfectly suited to analyse the frequency of contacts between sister DNA copies emerging from a replication fork. As a comparison, 3C-derived techniques cannot be used to map interactions between positions separated by less than 1500 bp (Lajoie et al., 2015; Mitter et al., 2020; Oomen et al., 2020).

We exploited the properties of two different recombinases, Cre, a self-active enzyme (Figure 1 to 7), and Xer, whose action is restricted to the immediate proximity of the cell division apparatus of bacteria after the onset of constriction (Figure 4). Using *V. cholerae* as a model, we showed that Cre-based f_{SC2} measurements reflect the relative duration of cohesion of newly-replicated DNA molecules behind replication forks (Figure 4) whereas Xer-based f_{SC2} measurements reflect the proximity of individualized sister-chromatids at the time of cell division (Figure 4). We further show that Cre-based f_{SC2} measurements unveil short-range locus-specific variations in cohesion, which had so far escaped detection by any other techniques (Figure 1, 2 and 7).

Cre-based f_{SC2} measurements also revealed that initiation and termination of replication of the two *V. cholerae* chromosomes take place in cohesive territories (Figure 2). In agreement, fluorescence microscopy observations suggested that sister copies of the origin region of the *E. coli* chromosome are highly cohesive (Bates and Kleckner, 2005; Joshi et al., 2013). However, we could have expected cohesion at the origin region of the *V. cholerae* chromosomes to be more limited than cohesion at the origin of the *E. coli* chromosome

because the *V. cholerae* chromosomes, as most other bacterial chromosomes and in contrast to the *E. coli* chromosome, are equipped with a partition machinery dedicated to the active segregation of sister origin copies (Fogel and Waldor, 2006; Yamaichi et al., 2007). The observation of the elevated cohesiveness of the replication origins of the *V. cholerae* chromosomes suggest that the partition machineries cannot release all of the cohesion links but only serve to assure the correct repositioning of sister origins in the cell after their individualisation. Furthermore, we found that the cohesiveness of the *ori2*-territory was not entirely lost in MCH1, in which *ori2* is deleted and in which the *ori2*-territory is split into two regions that are displaced to the middle of opposite chromosomal arms (Figure 4D). More strikingly, cohesion within the *dif1*-territory was as important in MCH1 as in the wild type context, even though *dif1* is deleted and the domain is split in two parts that are displaced to the middle of opposite chromosomal arms (Figure 4C). These results suggest that the local cohesiveness of sister chromatids is at least in part dictated by sequence-specific factors. However, we did not observe any obvious correlation between short-range variations in cohesion and the local base composition, methylation and transcriptional status of the chromosomes (Figure 7). These results suggest that multiple factors are at the origin of the local variations in cohesion along the length of chromosomes. We believe that Hi-SC2 will be a key asset to determine these factors and unravel their local relative contribution to cohesion. As an example, Hi-SC2 revealed that H-NS was responsible for the elevated cohesiveness of sister copies of VPI-1 in the middle of the left arm of Chr1 and of sister copies of the O-antigen region in the origin proximal part of Chr1 (Figure 5 and 6). The implication of a bacterial repressor in cohesion creates a parallel with the action of cohesins in eukaryotes, which ensure sister-chromatid cohesion but also participate in the regulation of transcription via the formation of topologically associated domains (Uhlmann, 2008).

Limitations

Cre is a self-active enzyme, which is widely used for genetic engineering in bacteria and eukaryotes (Murray et al., 2012). Several methodologies already exist that permit to induce the production of Cre at a specific time and/or specific stage of the cell cycle (Fernández-Chacón et al., 2019). Hi-SC2 experiments are easy to perform and the analysis and representation of the results is straight forward. Generation of a library of cells harbouring a SC2 reporter at a different location is probably the most time-consuming part of Hi-SC2. However, a few days are sufficient for any unicellular organism that can be isolated on plates such as bacteria or yeast. In the present study, we used a Mariner transposon for the introduction of the SC2 reporters. Mariner transposons target 5'-TA-3' sites, which might not be suited for GC-rich genomes. However, reporters can also be delivered using Tn5 and Mu transposons (Liu et al., 2018), LTR-retrotransposons (Maksakova et al., 2006) and gamma-retroviruses (Nusse, 1991).

Acknowledgements

We thank C. Possoz, G. Lelandais, V. Lioy and Y. Yamaichi and the high-throughput sequencing facility of the I2BC. The work was supported by the ERC (FP7/2007-2013, grant number 28159) and the ANR (grants 2016-CE12-0030-0 and 2018-CE12-0012-03).

Author contributions

E.E. and E.P. conducted the experiments. E.E. and FX.B. designed the experiments, analysed the results and wrote the paper.

Declaration of Interests

The authors declare no competing interests.

References

Adhikari, S., and Curtis, P.D. (2016). DNA methyltransferases and epigenetic regulation in bacteria. FEMS Microbiol Rev *40*, 575–591.

Amit, R., Oppenheim, A.B., and Stavans, J. (2003). Increased Bending Rigidity of Single DNA Molecules by H-NS, a Temperature and Osmolarity Sensor. Biophys J *84*, 2467–2473.

Ayala, J.C., Wang, H., Benitez, J.A., and Silva, A.J. (2015). RNA-Seq analysis and whole genome DNA-binding profile of the Vibrio cholerae histone-like nucleoid structuring protein (H-NS). Genom Data *5*, 147–150.

Baek, J.H., and Chattoraj, D.K. (2014). Chromosome I Controls Chromosome II Replication in Vibrio cholerae. PLoS Genet *10*, e1004184.

Bates, D., and Kleckner, N. (2005). Chromosome and Replisome Dynamics in E. coli: Loss of Sister Cohesion Triggers Global Chromosome Movement and Mediates Chromosome Segregation. Cell *121*, 899–911.

Chatterjee, S.N., and Chaudhuri, K. (2003). Lipopolysaccharides of Vibrio cholerae. I. Physical and chemical characterization. Biochim Biophys Acta *1639*, 65–79.

Chun, J., Grim, C.J., Hasan, N.A., Lee, J.H., Choi, S.Y., Haley, B.J., Taviani, E., Jeon, Y.-S., Kim, D.W., Lee, J.-H., et al. (2009). Comparative genomics reveals mechanism for short-term and long-term clonal transitions in pandemic Vibrio cholerae. Proc. Natl. Acad. Sci. U.S.A. *106*, 15442–15447.

David, A., Demarre, G., Muresan, L., Paly, E., Barre, F.-X., and Possoz, C. (2014). The two Cis-acting sites, parS1 and oriC1, contribute to the longitudinal organisation of Vibrio cholerae chromosome I. PLoS Genet. *10*, e1004448.

DeBoy, R.T., and Craig, N.L. (1996). Tn7 transposition as a probe of cis interactions between widely separated (190 kilobases apart) DNA sites in the Escherichia coli chromosome. J Bacteriol *178*, 6184–6191.

Dekker, J., Rippe, K., Dekker, M., and Kleckner, N. (2002). Capturing Chromosome Conformation. Science *295*, 1306–1311.

Demarre, G., Guérout, A.-M., Matsumoto-Mashimo, C., Rowe-Magnus, D.A., Marlière, P., and Mazel, D. (2005). A new family of mobilizable suicide plasmids based on broad host range R388 plasmid (IncW) and RP4 plasmid (IncPα) conjugative machineries and their cognate Escherichia coli host strains. Research in Microbiology *156*, 245–255.

Demarre, G., Galli, E., Muresan, L., Paly, E., David, A., Possoz, C., and Barre, F.-X. (2014). Differential management of the replication terminus regions of the two Vibrio cholerae chromosomes during cell division. PLoS Genet. *10*, e1004557.

Dorman, C.J. (2007). H-NS, the genome sentinel. Nature Reviews Microbiology *5*, 157–161.

Espeli, O., Mercier, R., and Boccard, F. (2008). DNA dynamics vary according to macrodomain topography in the E. coli chromosome. Mol. Microbiol. *68*, 1418–1427.

Espinosa, E., Barre, F.-X., and Galli, E. (2017). Coordination between replication, segregation and cell division in multi-chromosomal bacteria: lessons from Vibrio cholerae. Int. Microbiol. *20*, 121–129.

Fernández-Chacón, M., Casquero-García, V., Luo, W., Francesca Lunella, F., Ferreira Rocha, S., Del Olmo-Cabrera, S., and Benedito, R. (2019). iSuRe-Cre is a genetic tool to reliably induce and report Cre-dependent genetic modifications. Nat Commun *10*.

Fisher, J.K., Bourniquel, A., Witz, G., Weiner, B., Prentiss, M., and Kleckner, N. (2013). Four dimensional imaging of E. coli nucleoid organization and dynamics in living cells. Cell *153*, 882–895.

Fogel, M.A., and Waldor, M.K. (2006). A dynamic, mitotic-like mechanism for bacterial chromosome segregation. Genes Dev *20*, 3269–3282.

Galli, E., Poidevin, M., Le Bars, R., Desfontaines, J.-M., Muresan, L., Paly, E., Yamaichi, Y., and Barre, F.-X. (2016). Cell division licensing in the multi-chromosomal Vibrio cholerae bacterium. Nat Microbiol *1*, 16094.

Galli, E., Midonet, C., Paly, E., and Barre, F.-X. (2017). Fast growth conditions uncouple the final stages of chromosome segregation and cell division in Escherichia coli. PLoS Genet. *13*, e1006702.

Galli, E., Ferat, J.-L., Desfontaines, J.-M., Val, M.-E., Skovgaard, O., Barre, F.-X., and Possoz, C. (2019). Replication termination without a replication fork trap. Scientific Reports *9*, 8315.

Haering, C.H., Farcas, A.-M., Arumugam, P., Metson, J., and Nasmyth, K. (2008). The cohesin ring concatenates sister DNA molecules. Nature *454*, 297–301.

Hassan, F., Kamruzzaman, M., Mekalanos, J.J., and Faruque, S.M. (2010). Satellite phage TLCφ enables toxigenic conversion by CTX phage through dif site alteration. Nature *467*, 982–985.

Heidelberg, J.F., Eisen, J.A., Nelson, W.C., Clayton, R.A., Gwinn, M.L., Dodson, R.J., Haft, D.H., Hickey, E.K., Peterson, J.D., Umayam, L., et al. (2000). DNA sequence of both chromosomes of the cholera pathogen *Vibrio cholerae* . Nature *406*, 477–483.

Herrington, D.A., Hall, R.H., Losonsky, G., Mekalanos, J.J., Taylor, R.K., and Levine, M.M. (1988). Toxin, toxin-coregulated pili, and the toxR regulon are essential for Vibrio cholerae pathogenesis in humans. J Exp Med *168*, 1487–1492.

Higgins, N.P., Yang, X., Fu, Q., and Roth, J.R. (1996). Surveying a supercoil domain by using the gamma delta resolution system in Salmonella typhimurium. Journal of Bacteriology *178*, 2825–2835.

Hoess, R., Wierzbicki, A., and Abremski, K. (1985). Formation of small circular DNA molecules via an in vitro site-specific recombination system. Gene *40*, 325–329.

Javer, A., Long, Z., Nugent, E., Grisi, M., Siriwatwetchakul, K., Dorfman, K.D., Cicuta, P., and Lagomarsino, M.C. (2013). Short-time movement of E. coli chromosomal loci depends on coordinate and subcellular localization. Nat Commun *4*, 1–8.

Joshi, M.C., Bourniquel, A., Fisher, J., Ho, B.T., Magnan, D., Kleckner, N., and Bates, D. (2011). Escherichia coli sister chromosome separation includes an abrupt global transition with concomitant release of late-splitting intersister snaps. Proc Natl Acad Sci U S A *108*, 2765–2770.

Joshi, M.C., Magnan, D., Montminy, T.P., Lies, M., Stepankiw, N., and Bates, D. (2013). Regulation of sister chromosome cohesion by the replication fork tracking protein SeqA. PLoS Genet. *9*, e1003673.

Kennedy, S.P., Chevalier, F., and Barre, F.-X. (2008). Delayed activation of Xer recombination at dif by FtsK during septum assembly in Escherichia coli. Mol. Microbiol. *68*, 1018–1028.

Kleckner, N., Zickler, D., Jones, G.H., Dekker, J., Padmore, R., Henle, J., and Hutchinson, J. (2004). A mechanical basis for chromosome function. Proceedings of the National Academy of Sciences of the United States of America *101*, 12592–12597.

Lajoie, B.R., Dekker, J., and Kaplan, N. (2015). The Hitchhiker's Guide to Hi-C Analysis: Practical guidelines. Methods *72*, 65–75.

Lau, I.F., Filipe, S.R., Søballe, B., Økstad, O.-A., Barre, F.-X., and Sherratt, D.J. (2003). Spatial and temporal organization of replicating Escherichia coli chromosomes. Mol. Microbiol. *49*, 731–743.

Lazar-Stefanita, L., Scolari, V.F., Mercy, G., Muller, H., Guérin, T.M., Thierry, A., Mozziconacci, J., and Koszul, R. (2017). Cohesins and condensins orchestrate the 4D dynamics of yeast chromosomes during the cell cycle. The EMBO Journal *36*, 2684–2697.

Lesterlin, C., Gigant, E., Boccard, F., and Espéli, O. (2012). Sister chromatid interactions in bacteria revealed by a site-specific recombination assay. EMBO J. *31*, 3468–3479.

Li, H., and Durbin, R. (2010). Fast and accurate long-read alignment with Burrows–Wheeler transform. Bioinformatics *26*, 589–595.

Li, H., Handsaker, B., Wysoker, A., Fennell, T., Ruan, J., Homer, N., Marth, G., Abecasis, G., and Durbin, R. (2009). The Sequence Alignment/Map format and SAMtools. Bioinformatics *25*, 2078–2079.

Lieberman-Aiden, E., van Berkum, N.L., Williams, L., Imakaev, M., Ragoczy, T., Telling, A., Amit, I., Lajoie, B.R., Sabo, P.J., Dorschner, M.O., et al. (2009). Comprehensive mapping of long range interactions reveals folding principles of the human genome. Science *326*, 289–293.

Lioy, V.S., Cournac, A., Marbouty, M., Duigou, S., Mozziconacci, J., Espéli, O., Boccard, F., and Koszul, R. (2018). Multiscale Structuring of the E. coli Chromosome by Nucleoid-Associated and Condensin Proteins. Cell *172*, 771-783.e18.

Liu, H., Price, M.N., Waters, R.J., Ray, J., Carlson, H.K., Lamson, J.S., Chakraborty, R., Arkin, A.P., and Deutschbauer, A.M. (2018). Magic Pools: Parallel Assessment of Transposon Delivery Vectors in Bacteria. MSystems *3*.

Maksakova, I.A., Romanish, M.T., Gagnier, L., Dunn, C.A., van de Lagemaat, L.N., and Mager, D.L. (2006). Retroviral Elements and Their Hosts: Insertional Mutagenesis in the Mouse Germ Line. PLoS Genet *2*.

Mandlik, A., Livny, J., Robins, W.P., Ritchie, J.M., Mekalanos, J.J., and Waldor, M.K. (2011). RNA-seq-based monitoring of infection-linked changes in Vibrio cholerae gene expression. Cell Host Microbe *10*, 165–174.

Marinus, M.G., and Casadesus, J. (2009). Roles of DNA adenine methylation in host–pathogen interactions: mismatch repair, transcriptional regulation, and more. FEMS Microbiol Rev *33*, 488–503.

Martin, M. (2011). Cutadapt removes adapter sequences from high-throughput sequencing reads. EMBnet.Journal *17*, 10–12.

Meibom, K.L., Blokesch, M., Dolganov, N.A., Wu, C.Y., and Schoolnik, G.K. (2005). Chitin induces natural competence in Vibrio cholerae. Science *310*, 1824–1827.

Mercier, R., Petit, M.-A., Schbath, S., Robin, S., El Karoui, M., Boccard, F., and Espéli, O. (2008). The MatP/matS site-specific system organizes the terminus region of the E. coli chromosome into a macrodomain. Cell *135*, 475–485.

Midonet, C., Das, B., Paly, E., and Barre, F.-X. (2014). XerD-mediated FtsK-independent integration of TLCϕ into the Vibrio cholerae genome. Proc. Natl. Acad. Sci. U.S.A. *111*, 16848–16853.

Midonet, C., Miele, S., Paly, E., Guerois, R., and Barre, F.-X. (2019). The TLCΦ satellite phage harbors a Xer recombination activation factor. PNAS 201902905.

Mitter, M., Gasser, C., Takacs, Z., Langer, C.C.H., Tang, W., Jessberger, G., Beales, C.T., Neuner, E., Ameres, S.L., Peters, J.-M., et al. (2020). Sister-chromatid-sensitive Hi-C reveals the conformation of replicated human chromosomes. BioRxiv 2020.03.10.978148.

Morales, C., and Losada, A. (2018). Establishing and dissolving cohesion during the vertebrate cell cycle. Curr. Opin. Cell Biol. *52*, 51–57.

Murray, S.A., Eppig, J.T., Smedley, D., Simpson, E.M., and Rosenthal, N. (2012). Beyond knockouts: cre resources for conditional mutagenesis. Mamm Genome *23*, 587–599.

Nasmyth, K., and Haering, C.H. (2009). Cohesin: Its Roles and Mechanisms. Annual Review of Genetics *43*, 525–558.

Nolivos, S., Upton, A.L., Badrinarayanan, A., Müller, J., Zawadzka, K., Wiktor, J., Gill, A., Arciszewska, L., Nicolas, E., and Sherratt, D. (2016). MatP regulates the coordinated action of topoisomerase IV and MukBEF in chromosome segregation. Nat Commun *7*, 10466.

Nusse, R. (1991). Insertional Mutagenesis in Mouse Mammary Tumorigenesis. In Retroviral Insertion and Oncogene Activation, H.-J. Kung, and P.K. Vogt, eds. (Berlin, Heidelberg: Springer), pp. 43–65.

Oomen, M.E., Hedger, A.K., Watts, J.K., and Dekker, J. (2020). Detecting chromatin interactions along and between sister chromatids with SisterC. BioRxiv 2020.03.10.986208.

van Opijnen, T., Bodi, K.L., and Camilli, A. (2009). Tn-seq; high-throughput parallel sequencing for fitness and genetic interaction studies in microorganisms. Nat Methods *6*, 767–772.

Pritchard, J.R., Chao, M.C., Abel, S., Davis, B.M., Baranowski, C., Zhang, Y.J., Rubin, E.J., and Waldor, M.K. (2014). ARTIST: High-Resolution Genome-Wide Assessment of Fitness Using Transposon-Insertion Sequencing. PLoS Genet *10*.

Rasmussen, T., Jensen, R.B., and Skovgaard, O. (2007). The two chromosomes of Vibrio cholerae are initiated at different time points in the cell cycle. Embo J *26*, 3124–3131.

Rimsky, S., Zuber, F., Buckle, M., and Buc, H. (2001). A molecular mechanism for the repression of transcription by the H-NS protein. Molecular Microbiology *42*, 1311–1323.

Schalbetter, S.A., Goloborodko, A., Fudenberg, G., Belton, J.-M., Miles, C., Yu, M., Dekker, J., Mirny, L., and Baxter, J. (2017). Structural maintenance of chromosome complexes differentially compact mitotic chromosomes according to genomic context. Nat Cell Biol *19*, 1071–1080.

Sliusarenko, O., Heinritz, J., Emonet, T., and Jacobs-Wagner, C. (2011). High-throughput, subpixel precision analysis of bacterial morphogenesis and intracellular spatio-temporal dynamics. Molecular Microbiology *80*, 612–627.

Spurio, R., Falconi, M., Brandi, A., Pon, C.L., and Gualerzi, C.O. (1997). The oligomeric structure of nucleoid protein H-NS is necessary for recognition of intrinsically curved DNA and for DNA bending. EMBO J. *16*, 1795–1805.

Stouf, M., Meile, J.-C., and Cornet, F. (2013). FtsK actively segregates sister chromosomes in Escherichia coli. Proc. Natl. Acad. Sci. U.S.A. *110*, 11157–11162.

Trucksis, M., Michalski, J., Deng, Y.K., and Kaper, J.B. (1998). The Vibrio cholerae genome contains two unique circular chromosomes. Proc Natl Acad Sci U S A *95*, 14464–14469.

Uhlmann, F. (2008). Molecular biology: Cohesin branches out. Nature *451*, 777–778.

Val, M.-E., Bouvier, M., Campos, J., Sherratt, D., Cornet, F., Mazel, D., and Barre, F.-X. (2005). The single-stranded genome of phage CTX is the form used for integration into the genome of Vibrio cholerae. Mol. Cell *19*, 559–566.

Val, M.-E., Kennedy, S.P., El Karoui, M., Bonné, L., Chevalier, F., and Barre, F.-X. (2008). FtsK-dependent dimer resolution on multiple chromosomes in the pathogen Vibrio cholerae. PLoS Genet. *4*, e1000201.

Val, M.-E., Skovgaard, O., Ducos-Galand, M., Bland, M.J., and Mazel, D. (2012). Genome Engineering in Vibrio cholerae: A Feasible Approach to Address Biological Issues. PLoS Genet *8*.

Val, M.-E., Marbouty, M., de Lemos Martins, F., Kennedy, S.P., Kemble, H., Bland, M.J., Possoz, C., Koszul, R., Skovgaard, O., and Mazel, D. (2016). A checkpoint control orchestrates the replication of the two chromosomes of Vibrio cholerae. Science Advances *2*, e1501914–e1501914.

Valens, M., Penaud, S., Rossignol, M., Cornet, F., and Boccard, F. (2004). Macrodomain organization of the Escherichia coli chromosome. Embo J *23*, 4330–4341.

Vickridge, E., Planchenault, C., Cockram, C., Junceda, I.G., and Espéli, O. (2017). Management of E. coli sister chromatid cohesion in response to genotoxic stress. Nat Commun *8*.

Waldor, M.K., and Mekalanos, J.J. (1996). Lysogenic conversion by a filamentous phage encoding cholera toxin. Science *272*, 1910–1914.

Walker, D.M., Freddolino, P.L., and Harshey, R.M. (2020). A Well-Mixed E. coli Genome: Widespread Contacts Revealed by Tracking Mu Transposition. Cell *180*, 703-716.e18.

Wang, X., Reyes-Lamothe, R., and Sherratt, D.J. (2008). Modulation of Escherichia coli sister chromosome cohesion by topoisomerase IV. Genes Dev. *22*, 2426–2433.

Yamaichi, Y., Iida, T., Park, K.-S., Yamamoto, K., and Honda, T. (1999). Physical and genetic map of the genome of Vibrio parahaemolyticus: presence of two chromosomes in Vibrio species. Molecular Microbiology *31*, 1513–1521.

Yamaichi, Y., Fogel, M.A., and Waldor, M.K. (2007). par genes and the pathology of chromosome loss in Vibrio cholerae. Proc Natl Acad Sci U S A *104*, 630–635.

FIGURE LEGENDS

Figure 1. Overview of Hi-SC2. (A) Schematic representation of the assay, see also Figure S1. The SC2 reporter (black circle) consists of two directly repeated site-specific recombination (SRR) sites (purple triangles), separated by a very short piece of DNA. When the cognate tyrosine recombinase is produced (y-rec), intermolecular recombination events between sister copies of the SC2 reporter can lead to the formation of a copy with a single SSR site on one of the two sister chromatids and a copy with three SSR sites on the other chromatid, which is subsequently converted into a copy with a single recombination site by intramolecular recombination. High-throughput paired-end sequencing permits to determine the genomic position of the SC2 reporter (orange primer) and whether it contains a single SSR site (black primer). The proportion of reporter with single SSR site to the total number of SC2 reporter inserted at a given genomic position, x, reflects the frequency of sister chromatid contacts at this position, $f_{SC2}(x)$. (B) Cre-based f_{exc} profiles along *V. cholerae* Chr1 and Chr2. Blue and green lines: 10 kbp sliding-window profiles along Chr1 and Chr2, respectively; orange and pink lines: 100 kbp sliding-window profiles along Chr1 and Chr2, respectively. Solid and open circles depict the origin and terminus of replication of the chromosomes, respectively; the left and right replication arms are indicated as L and R, respectively. Left bottom panel: Zoom of the 1 kbp excision profile around the region of insertion of Cre (from position 588 to 614 kbp). Right bottom panel: Zoom of the frequency of excision around the region of insertion of Cre (from position 598254 to 604418 bp),

showing f_{exc} at each insertion of the reporter. As expected, no excision is observed for the reporters inserted in *cre* and *araC* genes.

Figure 2. Short and long *loxP* cassettes excision exclusively result from Cre-mediated recombination events. (A) Comparison of the f_{exc} profiles of short (SC2 reporter, FX221 to FX224 datasets) and long *loxP* cassettes (Cre-activity reporter, FX226 and FX227 datasets) at different time points after induction of Cre-production. Blue and green lines: short *loxP* cassette f_{exc} profiles along Chr1 and Chr2, respectively; orange and pink lines: long *loxP* cassette f_{exc} profiles along Chr1 and Chr2, respectively. Right y-axis: short cassette f_{exc} scale; left y-axis: long cassette f_{exc} scale. Bottom right: scheme of the Cre-mediated intramolecular excision events mediated by Cre on long *loxP* cassettes. (B) Reproducibility of Hi-SC2. Blue and green lines: short *loxP* cassette f_{exc} profiles obtained after 90' of Cre induction (FX224 dataset) along Chr1 and Chr2, respectively; orange and pink lines: short *loxP* cassette f_{exc} profile obtained for a second transposition library under the same experimental conditions (FX239 dataset) along Chr1 and Chr2, respectively; black lines: 100 kbp sliding-window f_{exc} profiles of FX224 and FX239. The f_{exc} profiles of FX239 dataset are slightly higher than the f_{exc} profiles of the FX224 dataset, which probably reflects a difference of growth between the two experiments. However, long- and short-distance variations were almost identical. See also Figure S2.

Figure 3. The excision of short *loxP* cassettes results from intermolecular recombination events between sister chromatids. (A) Schematic representation of the effect of rifampicin on the replication program in an asynchronous population of V. *cholerae* cells. Left, middle and right columns: scheme of Chr1 (blue) and Chr2 (green) in cells in three different replicative states before rifampicin addition, at two different times after rifampicin addition. Grey mark represents the *crtS* site. The chromosomal regions that will be eventually replicated are highlighted in orange and pink. (B) Upper panel: Chr1 (orange) and Chr2 (pink)

Cre-based Hi-SC2 profiles obtained in the presence of rifampicin in slow growth conditions (FX516 to FX519 datasets). As a comparison, we show the Chr1 (orange) and Chr2 (pink) Cre-based Hi-SC2 profiles obtained after 60' of induction in the absence of rifampicin. Bottom panels: Zoom of the Hi-SC2 profiles around *dif1*, *ori1*, *dif2* and *ori2* regions. See also Figure S3.

Figure 4. Relative cohesiveness of sister chromatids during the cell cycle. (A) Schematic representation of the choreography of segregation of Chr1 (blue) and Chr2 (green) in wild-type (WT) *V. cholerae* cells. Legend as in Figure 1B. (B) Schematic representation of the choreography of segregation of the unique chromosome of MCH1 *V. cholerae* cells. Chr2 (pink) is inserted at the *dif1* site of Chr1 (orange). (C) Cre-based f_{SC2} Hi-SC2 of the MCH1 chromosome (FX213 dataset). (D) Comparison of the Cre-based Hi-SC2 profiles of the *dif1* region in WT (FX224 dataset) and MCH1 (FX213 dataset) cells. (E) Comparison of the Cre-based Hi-SC2 profiles of the *ori2* region in WT (FX224 dataset) and MCH1 (FX213 dataset) cells. (F) Comparison of Cre-based (FX224 dataset) and Xer-based (FX129 dataset) Hi-SC2 profiles. Cre permits to monitor the f_{SC2} from the time of replication of a genomic position to the time of separation of the resulting sister copies. Xer permits to specifically monitor the f_{SC2} during septum constriction. See also Figure S4.

Figure 5. A highly cohesive territory surrounds the VPI-1 Vibrio pathogenicity island. (A) Comparison of the Cre-based Hi-SC2 profiles in WT (blue and green) and ΔVPI-1 cells (orange and pink). The position of VPI-1 is indicated with a grey box (from 2176653 to 2217966 bp). (B-D) Fluorescence microscopy analysis of the order of segregation of two neighbouring loci on the same replication arm. The schematic representation of the strains used for microscopy analysis is shown in (B). Origin- and terminus-proximal loci are depicted in green and purple, respectively. Distances between markers are indicated. The graphs in (C) show the mean and standard deviation of the relative proportion of cells with the indicated

number of foci observed in two sets of independent microscopy experiments. We analysed >1000 cells per strain per experiment. The two informative cell categories, i.e. the cells with 1 L1 and 2 L2 foci (1:2) and the cells with 2 L1 and 1 L2 foci (2:1), are highlighted in green and red, respectively. The relative proportion of cells in the different cell categories obtained in each set of individual experiment is shown in Figure S5. The graph in (D) shows the mean and standard deviation of the ratio between the number of cells in the 1:2 category and the number of cells in the 2:1 category in the three strains obtained in the two sets of independent microscopy experiments. *: the difference is statistically different (Fisher test, p-value < 0.001); n.s.: the difference is not statistically significant (Fisher test, p-value > 0.5). Equivalent significance results were obtained using the data of each individual set of microscopy experiments (Figure S5).

Figure 6. H-NS extends the cohesiveness of sister chromatids within VPI-1 and the O-antigen region. (A) Upper panel: Cre-based Hi-SC2 profiles in WT (blue and green) and Δ*hns* cells (orange and pink); Lower panel: relative distribution of H-NS along the *V. cholerae* genome analysed by ChIP-seq (Ayala et al., 2015). Grey arrows indicate regions of significantly lower SC2 frequencies in Δ*hns* cells. (B) Correlation between the SC2-reporter cassette excision frequencies in Δ*hns* (FX215 dataset) and WT cells (FX224 dataset). Black line: linear regression of the Δ*hns* and WT data. Left panel: data points within VPI-1 and the 2160 to 2283 kbp origin-proximal part of the VPI-1 territory are highlighted in blue and green, respectively; Right panel: data points within the 2825477 to 2839408 bp O-antigen region are highlighted in orange. Regions containing highlighted domains are enlarged. See also Figure S6.

Figure 7. Hi-SC2 unveils small short-distance locus variations over the whole genome. (A) Comparison of small short-distance locus variations in the f_{exc} of short *loxP* cassettes. To facilitate the visualization of the small-locus variations, long-distance variations in the f_{exc}

were subtracted from the Hi-SC2 profiles. Blue and green lines: FX244 dataset profiles along Chr1 and Chr2, respectively; Orange and pink lines: FX239 dataset profiles along Chr1 and Chr2, respectively; left y-axis: scale of the FX224 dataset profiles; right y-axis: scale of the FX239 dataset profiles. (B) 10 kbp sliding window profile of the GC content along the *V. cholerae* genome (%). (C) 10 kbp sliding window profile of the number of GACT sites along the *V. cholerae* genome (per thousands). (D) 10 kbp sliding window profile of the relative number of transcripts (log2) along the *V. cholerae* genome under slow growth conditions (Adapted from (Mandlik et al., 2011)).

RESOURCE AVAILABILITY

Lead Contact

Further information and requests for resources and reagents should be directed to and will be fulfilled by the Lead Contact, François-Xavier Barre (francois-xavier.barre@i2bc.paris-saclay.fr).

Materials Availability

All unique/stable reagents generated in this study are available from the Lead Contact with a completed Materials Transfer Agreement.

Data and Code Availability

Hi-SC2 data are available in the ArrayExpress database (http://www.ebi.ac.uk/arrayexpress) under accession number E-MTAB-8946. Fluorescence microscopy images are accessible on Mendeley Data, V1, doi: 10.17632/wvnjh3hw4x (https://data.mendeley.com/datasets/wvnjh3hw4x/draft?a=5e43b973-7687-4fca-b3fa-d61dcde477bb). MatLab scripts used to generate the figures are available on request.

EXPERIMENTAL MODEL AND SUBJECT DETAILS

The El Tor N16961 *Vibrio cholerae* isolate was used as the experimental model (Heidelberg et al., 2000).

METHOD DETAILS

Strains and bacterial growth conditions. All the El Tor N16961 derivatives used in the study were constructed by natural transformation (Meibom et al., 2005). The are listed in Table S5. Strains were grown in LB at 37° C for fast growth conditions or M9 media supplemented with 0.2% fructose at 30°C for slow growth conditions.

Plasmids and oligonucleotides. Plasmids and oligonucleotides are listed in Table S6 and Table S7, respectively.

Cre- and Xer-based SC2 reporters. Cre and Xer are topologically independent recombinases, i.e. they can recombine sites belonging to different molecules, recombine sites directly repeated on the same molecule and sites in inverted orientations. The Cre- and Xer-based SC2 reporters consist of DNA cassettes flanked by two directly-repeated *loxP* or *dif1* sites, respectively. The recombination sites were separated by 21 bp in the case of *loxP* and 27 bp in the case of *dif* to prevent their excision by intramolecular recombination.

Cre-activity reporter. The Cre-activity reporter consists of a DNA cassette flanked by two directly-repeated *loxP* sites separated by 205 bp, which permits excision by intramolecular recombination.

Tightly inducible Cre and Xer production alleles. To ensure no leaky production of Cre or Xer, the recombinase genes were placed under the control of the arabinose promoter (P_{BAD}) and the *E. coli lacZ* promoter was inserted at the end of the gene in inverse orientation ($invP_{lac}$). Transcription from $invP_{lac}$ inhibits leaky transcription from P_{BAD} in the absence of arabinose. IPTG was added to all cultures to ensure $invP_{lac}$ transcription before the time of induction of the recombinases. To further ensure no leaky production, the Cre and Xer production alleles were inserted as a single copy in the *V. cholerae* genome.

Reporter library construction. The Cre- and Xer-based SC2 reporters and the Cre-activity reporter were randomly inserted by transposition. The transposition plasmids used to insert

the Cre- and Xer-based SC2 reporters and the Cre-activity reporter are derivatives of the pSWT23 suicide plasmid conjugation vector (Demarre et al., 2005). They carry the transposase of the *magellan5* Mariner transposon and a kanamycin resistance marker flanked by the inverted repeats of the transposon (*Himar*) in which a *Mme*I restriction site has been inserted to facilitate the analysis of the position of insertion of the kanamycin cassette by high-throughput sequencing (van Opijnen et al., 2009). The Rd2SP sequence (Illumina) was introduced downstream of the kanamycin resistance for sequencing purposes. The Cre- and Xer-based SC2 reporters and the Cre-activity reporter were cloned downstream of the Rd2SP sequence. The transposition vectors were introduced by conjugation as follows: donor (EE14 for the Cre-based SC2 reporter and Cre-activity reporter; EE6 for the Xer-based SC2 reporter) and recipient cells were grown for 16 hours at 37 °C in LB. The donor was grown with DAP (0.3 mM) and chloramphenicol (25 μg/ml) whereas the recipient was grown with zeocin (25 μg/ml) and IPTG (0.1 mM). 250 μl of each culture were mixed, washed in LB with IPTG, resuspended into 30 μl of LB with IPTG and placed into a 0.45μm filter (Millipore) in a LB agar plate supplemented with DAP and IPTG. Conjugation was carried out for 4 hours at 37°C. Thirty conjugations were performed per each library. After conjugations, cells were pooled together, resuspended in 6 ml of LB with IPTG and plated on LB plates containing kanamycin (50 μg/ml) and IPTG. Plates were incubated for 16 hours at 30 °C except for EEV113 and EEV114, which were incubated for 40 hours. Cells were scraped, mixed in LB with IPTG and stored in aliquots at -80 °C.

Hi-SC2 assays. Aliquots of the transposon library were thawed on ice and ~10^9 cells were diluted into 100 ml of media supplemented with IPTG. Cells were grown until exponential phase (OD_{600} 0.2). Then, ~10^9 cells were centrifuged and transferred into 10 ml of fresh media without IPTG. After 30 minutes, arabinose was added at a final concentration of 0.02%. ~10^9 cells were recovered and frozen in liquid nitrogen at different time points after induction. For

the replication arrest assay, rifampicin (300 µg/ml) was added 10 minutes after the induction of the expression of the recombinase. For the essential gene analysis, cells were collected after 24 hours (FX409 and FX410 datasets).

Paired-end sequencing. Extraction of chromosomal DNA was performed using the Sigma GenElute bacterial genomic DNA kit. 2 µg of DNA were digested for 4 hours with *Mme*I (NEB) following the manufacturer's instructions. Digested DNA was purified with MiniElute columns (Qiagen). The Pippinprep (SAGE science) was used to purify digested fragments of a length comprised between 800 bp and 2 kbp, which corresponds to the region containing the transposon. 400 ng of purified DNA was ligated overnight at 16 °C to adapters (Table S4) with T4 DNA ligase (NEB). Ligated DNA was purified using MiniElute columns (Qiagen). For each library, 3 PCR reactions were performed using Phusion polymerase (Thermofisher Scientific), 2 µl of ligated DNA as template and a pair of Illumina oligos (Table S4, P5 and P7). The PCR reactions were performed using the following parameters: 98 °C for 30 seconds, 17 cycles of 98 °C 30 seconds, 68 °C 30 seconds, 72 °C 30 seconds and a final step of 72 °C for 7 minutes. PCR products were concentrated with a MiniElute columns (Qiagen) and purified using Pippin Prep (SAGE science). Paired-end sequencing was performed on a NextSeq 500 (Illumina).

Sequencing run analysis. First, barcodes and adapter sequences were removed from the sequences using Cutadapt (Martin, 2011). Second, Cutadapt was used to remove the transposon end sequence. Third, Cutadapt was used to select total reads and reads in which the reporter cassette had been excised. Finally, the BWA software was used for the alignment of reads on genomes (Li and Durbin, 2010) and stored in the SAM format (Li et al., 2009). Reads obtained for WT, ΔHNS and ΔVPI-1 strains were aligned on the *V. cholerae* EEV29 genome for easy comparison. Reads obtained for EEV104 were aligned on the *V. cholerae* EEV104 genome and on the EEV29 genome for comparison.

Hi-SC2 and Cre-activity analysis. Unless otherwise stated, f_{exc} was calculated as the ratio between the number of single SSR sites over a 10 kbp window around the position and the total number of transposition insertion in this window. Note, however, that f_{exc} can also be monitored for each individual insertion of the reporter (Figure S1). Hi-SC2 profiles were calculated using MatLab (Mathworks).

Essential genes analysis. Essential genes and intergenic regions were determined using ARTIST (Pritchard et al., 2014). Results are shown in Table S6.

Fluorescence microscopy analysis. To confirm that the elevated frequency of cassette excision within the VPI-1 domain corresponded to a local increase in cohesion, we tagged a locus in the VPI-1 domain, just downstream of the pathogenicity island itself, L1, and a locus outside of the VPI-1 domain, L2, 80 kbp downstream of L1. As a control, we tagged two loci on the right replication arm of Chr1, R1 and R2, at a similar distance from *ori1* than L1 and L2, respectively. Hi-SC2 analysis suggested that the cohesiveness of sister R1 and R2 copies were similar. L1 and R1 were tagged with a *parSPMT1* site. L2 and R2 were tagged with a 3 kbp *lacO* array. The positions and numbers of L1 and R1 foci were visualized with a $ParB_{PMT1}$-YGFP fusion (David et al., 2014; Stouf et al., 2013) and the positions and numbers of L2 and R2 loci were visualized with a LacI-mCherry fusion (Lau et al., 2003). Differences in timing of segregation under slow growth were determined by calculating the proportion of cells displaying 1 YGFP and 1 mCherry foci (1:1), 2 YGFP and 1 mCherry foci (2:1), 1 YGFP and 2 mCherry foci (1:2) and 2 YGFP and 2 mCherry foci (2:2). Cells from the 1:1 and 2:2 categories are not informative. However, the proportion of cells belonging to the 2:1 and 1:2 categories reflect the difference in timing of separation of sister DNA copies at the two loci (Stouf et al., 2013). Cells from the 1:2 or 2:1 category are not very abundant, which imposed the analysis of >1000 cells. Cells were grown in M9 media supplemented with fructose as described in the reporter cassette excision assays. Cells were placed on an agarose

pad (1% w/v) (Ultrapure, Invitrogen). For snapshot analysis, cells images were acquired using a DM6000-B (Leica) fluorescence microscope equipped with an ORCA-Flash 4.0 camera (Hamamatsu) and piloted with MetaMorph (Version 7.8.8.0, Molecular Devices). They were analysed using MicrobeTracker (Sliusarenko et al., 2011).

QUANTIFICATION AND STATISTICAL ANALYSIS

We used the Fisher test to determine the significance of the differences between the ratio of the number of cells in the 1:2 category to the number of cells in the 2:1 category shown in Figure 5 and Figure S5.

ADDITIONAL RESSOURCES

Detailed protocol

Bench protocols for the generation of a library of reporter cells, performing the Hi-SC2 assays and paired-end sequencing and sequencing run analysis is supplied in Method S1.

KEY RESOURCES TABLE

REAGENT or RESOURCE	SOURCE	IDENTIFIER
Bacterial and Virus Strains		
Vibrio cholerae O1 biovar El Tor str. N16961	(Heidelberg et al., 2000).	NCBI: txid243277
N16961 *ChapR* Δ*lacZ* P_{BAD}-*xerC*-invP_{lac}-*aadA1* $Spec^R$, Gm^R	(Demarre et al., 2014)	GDV28
DH5α λpir	Lab stock	DH5α λpir
(F^-) RP4-2-Tc::Mu DAP^- Kan^R	(Demarre et al., 2005)	β2163
Chemicals, Peptides, and Recombinant Proteins		
MmeI	NEB	https://www.neb-online.fr/
T4 DNA ligase	NEB	https://www.neb-online.fr/
Phusion polymerase	Thermofisher Scientific	https://www.thermofisher.com
Critical Commercial Assays		
MinElute PCR Purification Kit	Qiagen	https://www.qiagen.com
Pippin Prep	SAGE science	https://sagescience.com/
NextSeq 500	Illumina	https://www.illumina.com/
Deposited Data		

Raw and analyzed sequencing data	This paper	https://www.ebi.ac.uk/arrayexpress/experiments/E-MTAB-
Fluorescence images	This paper	https://data.mendeley.com/
Recombinant DNA		
Ori R6K Cm^R conjugative vector	(Demarre et al., 2005)	pSW23T
magellan5 mini-transposon with engineered Mme I sites in the inverted repeats	(van Opijnen et al., 2009)	*magellan6*
Software and Algorithms		
Cutadapt	(Martin, 2011)	https://pypi.org/project/cutadapt/
BWA	(Li and Durbin, 2010)	http://bio-bwa.sourceforge.net
Samtools	(Li et al., 2009)	http://www.htslib.org/
MatLab	Mathworks	mathworks.com
MicrobeTracker	(Sliusarenko et al., 2011)	http://microbetracker.org/
ARTIST	(Pritchard et al., 2014)	https://doi-org.insb.bib.cnrs.fr/10.1371/journal.pgen.1004782.s001
Other		
Bench Protocol	This study	Method S1

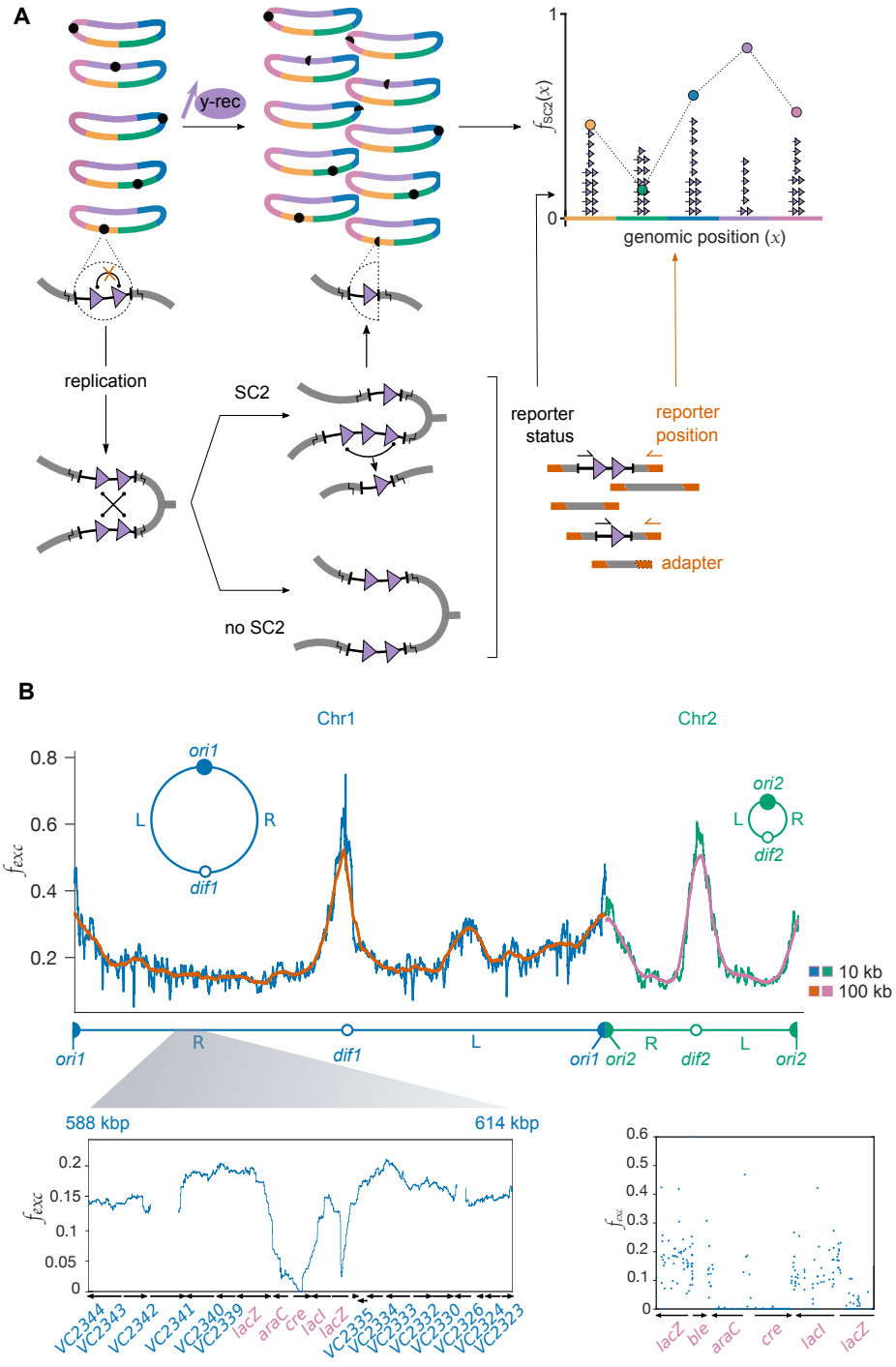
A
y-rec
replication
SC2
no SC2
reporter status
reporter position
adapter
genomic position (x)
B
Chr1
Chr2
ori1
dif1
ori2
dif2
10 kb
100 kb
588 kbp
614 kbp

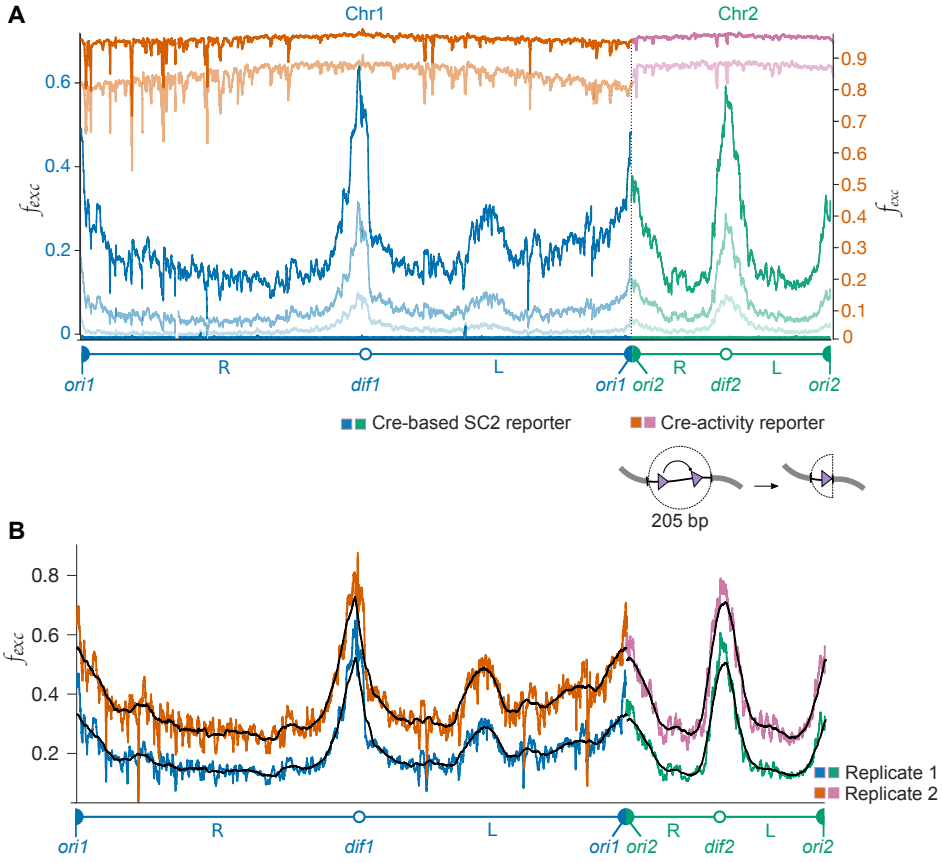
A
Chr1
Chr2
0.6
0.4
0.2
0
fexc
0.9
0.8
0.7
0.6
0.5
0.4
0.3
0.2
0.1
0
fexc
R
L
R
L
ori1
dif1
ori1 ori2
dif2
ori2
Cre-based SC2 reporter
Cre-activity reporter
205 bp

B
0.8
0.6
0.4
0.2
fexc
Replicate 1
Replicate 2
R
L
R
L
ori1
dif1
ori1 ori2
dif2
ori2

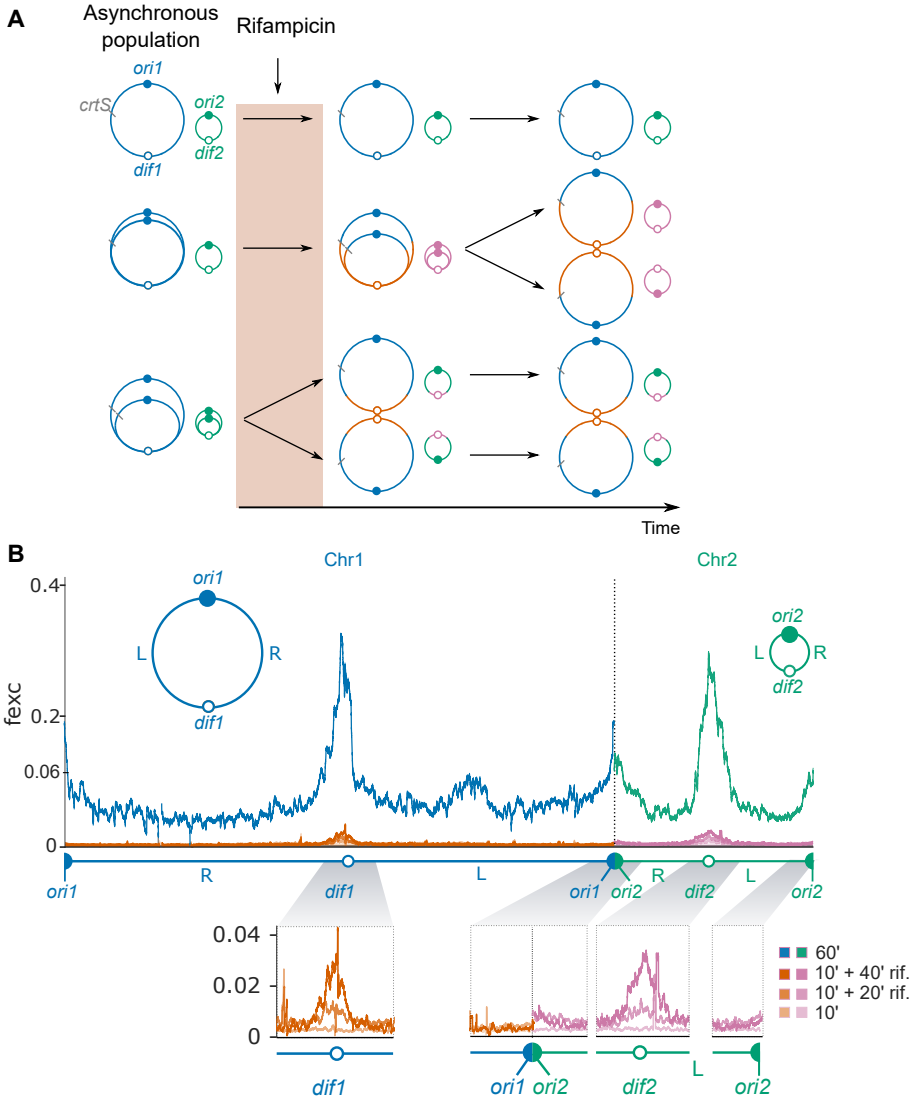
A
Asynchronous population
Rifampicin
ori1
crtS
ori2
dif2
dif1
Time
B
Chr1
Chr2
0.4
0.2
0.06
0
fexc
ori1
L
R
dif1
ori2
dif2
0.04
0.02
60'
10' + 40' rif.
10' + 20' rif.
10'

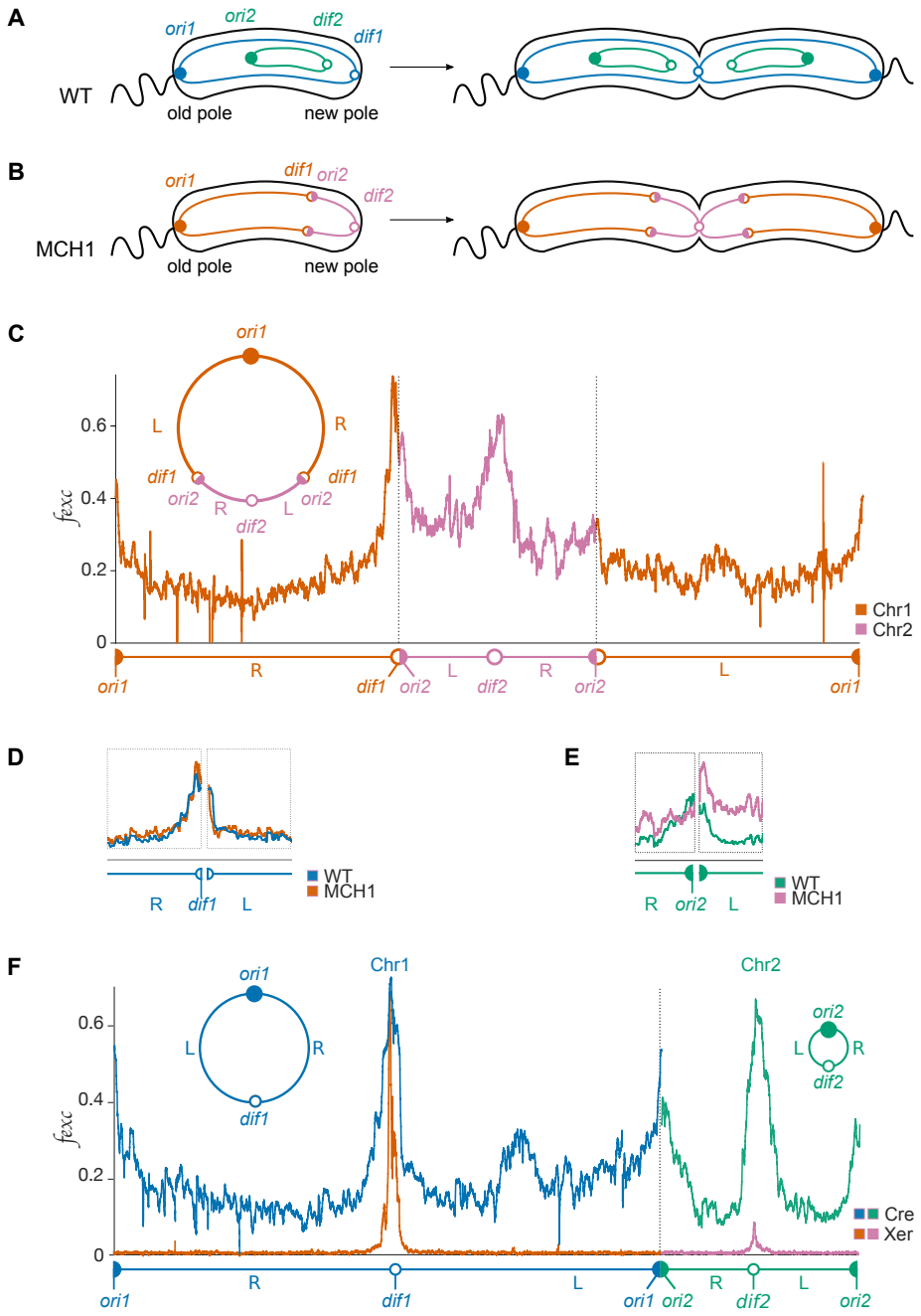
A
ori1
ori2
dif2
dif1
WT
old pole
new pole
B
ori1
dif1
ori2
dif2
MCH1
old pole
new pole
C
ori1
L
R
dif1
dif1
ori2
R
L
ori2
dif2
0.6
0.4
0.2
0
fexc
Chr1
Chr2
ori1
R
dif1
ori2
L
dif2
R
ori2
L
ori1
D
R
dif1
L
WT
MCH1
E
R
ori2
L
WT
MCH1
F
ori1
L
R
dif1
Chr1
Chr2
ori2
L
R
dif2
0.6
0.4
0.2
0
fexc
Cre
Xer
ori1
R
dif1
L
ori1
ori2
R
dif2
L
ori2

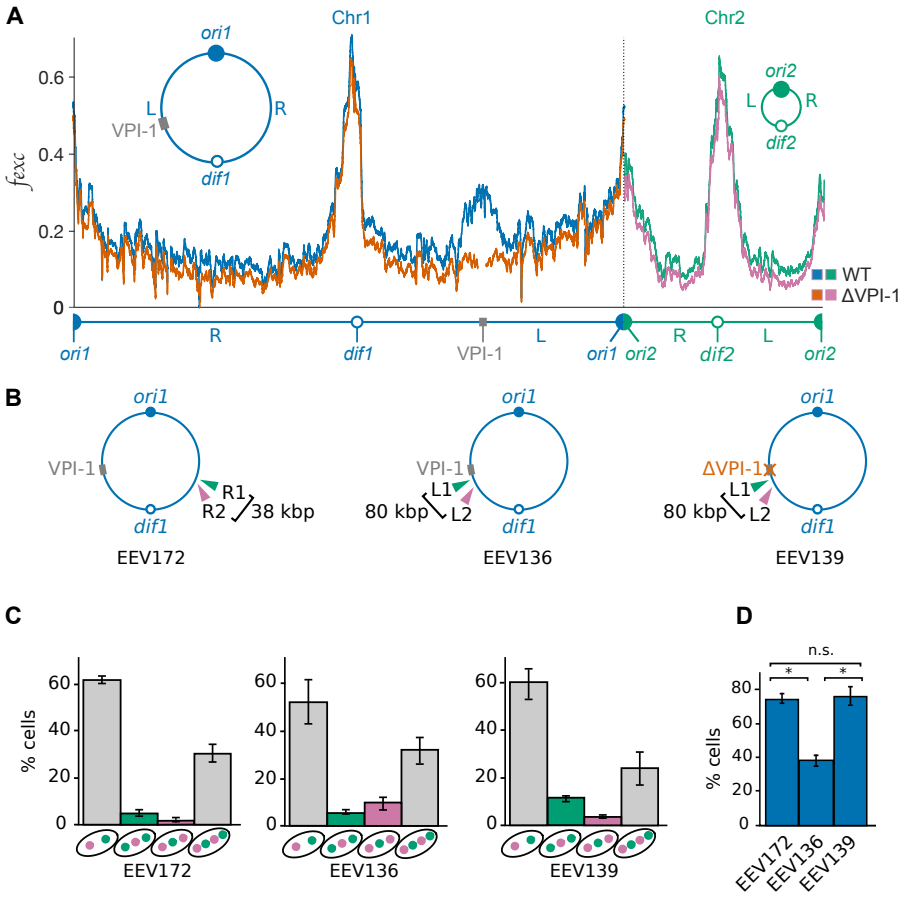
A
Chr1
Chr2
ori1
dif1
VPI-1
L
R
ori2
dif2
fexc
0.6
0.4
0.2
0
WT
ΔVPI-1
B
EEV172
EEV136
EEV139
R1
R2
38 kbp
80 kbp
L1
L2
ΔVPI-1
C
% cells
60
40
20
0
D
n.s.
*
80
60
40
20
0
EEV172
EEV136
EEV139

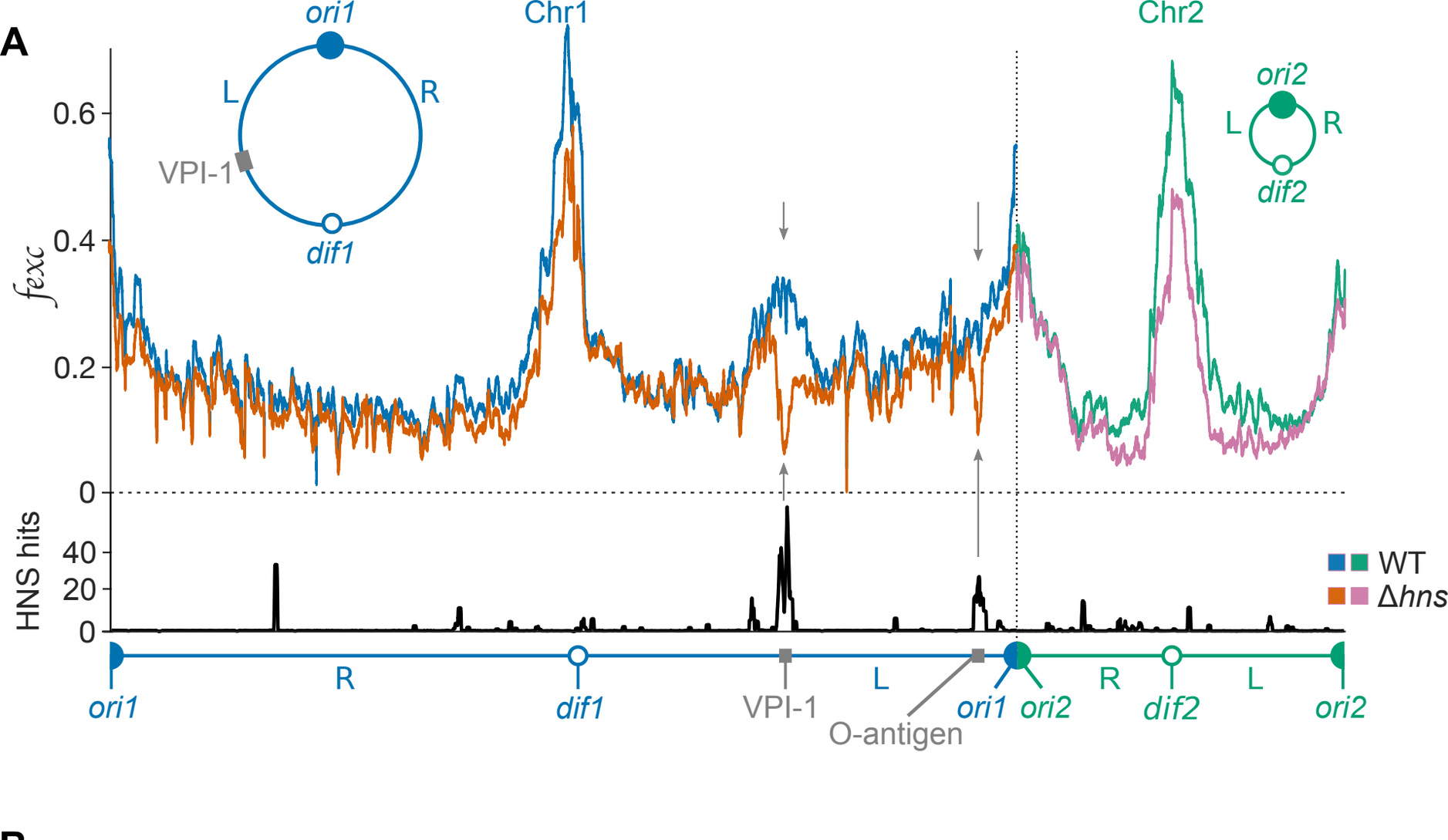
A
ori1
Chr1
Chr2
ori2
L
R
VPI-1
dif1
dif2
fexc
0.6
0.4
0.2
0
HNS hits
40
20
0
WT
Δhns
R
L
R
L
ori1
dif1
VPI-1
ori1
ori2
dif2
ori2
O-antigen

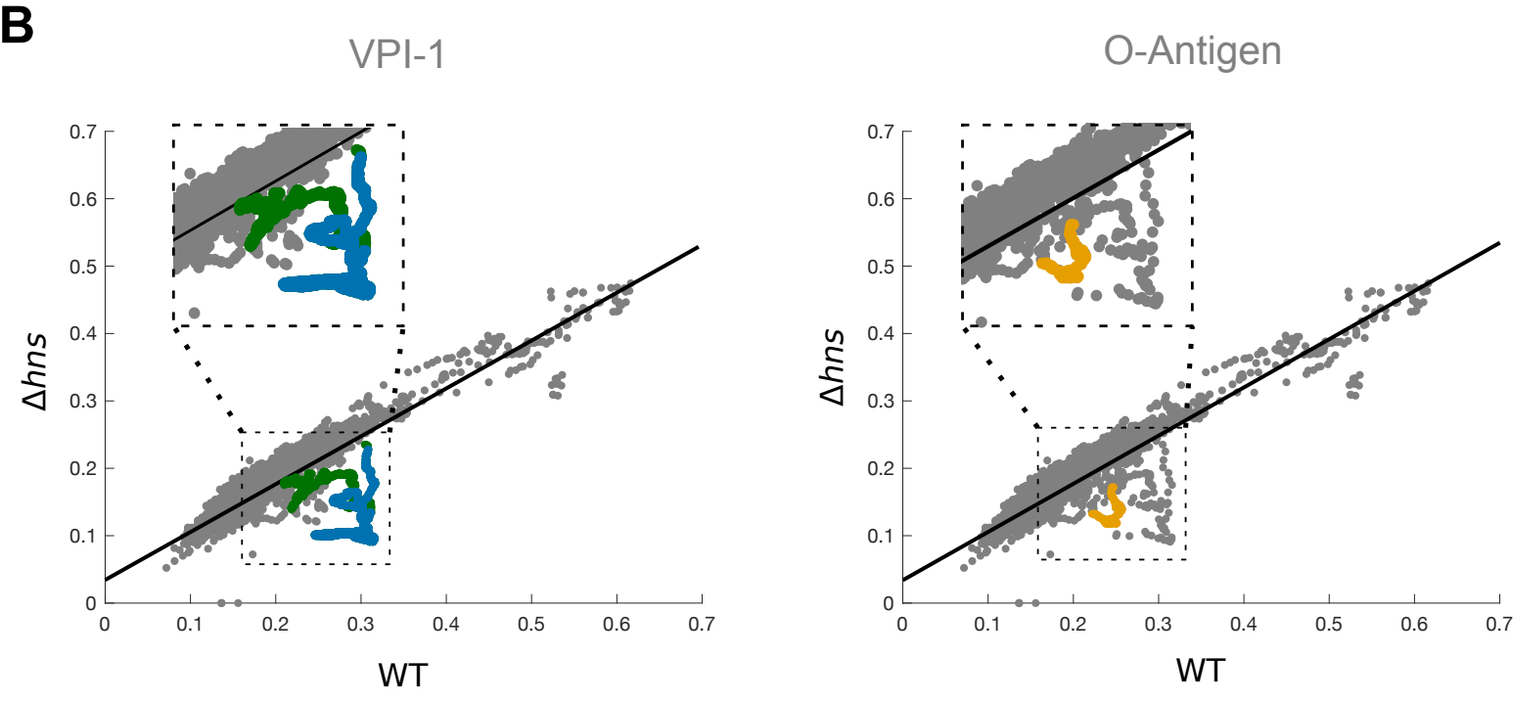
B
VPI-1
O-Antigen
Δhns
WT
0
0.1
0.2
0.3
0.4
0.5
0.6
0.7

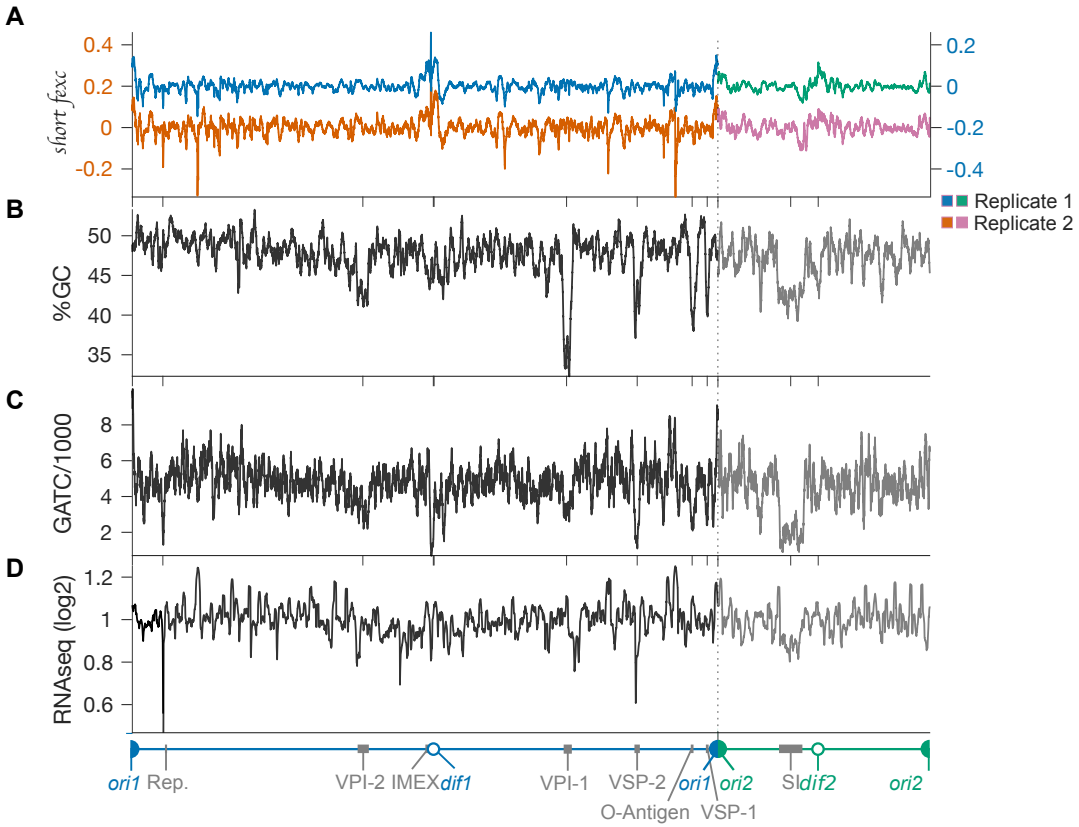
A
B
C
D
short fexc
0.4
0.2
0
-0.2
0.2
0
-0.2
-0.4
Replicate 1
Replicate 2
%GC
50
45
40
35
GATC/1000
8
6
4
2
RNAseq (log2)
1.2
1
0.8
0.6
ori1 Rep.
VPI-2
IMEX
dif1
VPI-1
VSP-2
O-Antigen
ori1
ori2
VSP-1
SI
dif2
ori2

-

Hi-SC2: a high-resolution whole-genome methodogy to analyse cohesion

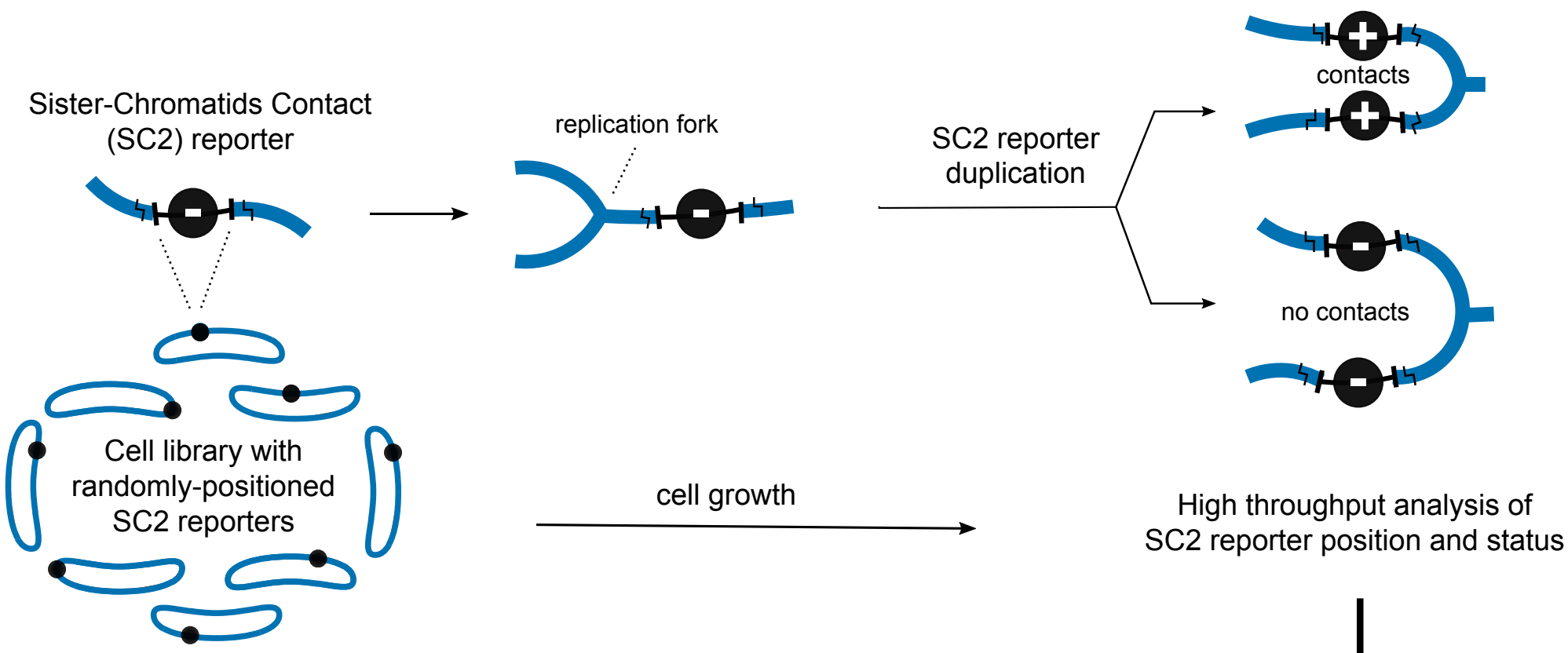

Application to Vibrio cholerae

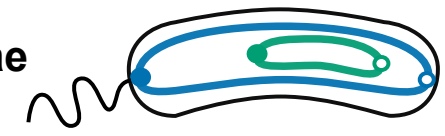

	Cohesion	
	WT	*Δhns*
ori1	+	+
dif1	+	+
VPI-1	+	-
ori2	+	+
dif2	+	+

+: high; -: low